Ground- and Excited-State Structure and Spin State of a Nickel-Bipyridine Photocatalyst Revealed by X-ray Absorption Spectroscopy

Rachel F. Wallick[1], Sagnik Chakrabarti[1], John H. Burke[1], Richard Gnewkow[2,3], Ju Byeong Chae[1], Thomas C. Rossi[2], Ioanna Mantouvalou[2,3], Birgit Kanngießer[2,3], Mattis Fondell[2], Sebastian Eckert[2], Conner Dykstra[1], Laura E. Smith[1], Josh Vura-Weis[1]*, Liviu M. Mirica[1]*, Renske M. van der Veen[1,2,3]*

[1]Department of Chemistry, University of Illinois at Urbana-Champaign, Urbana, Illinois, 61801, USA

[2]Helmholtz Center Berlin for Materials and Energy, Berlin, 12489, Germany

[3]Institute of Optics and Atomic Physics, Technische Universität Berlin, Berlin, 10623, Germany

*vuraweis@illinois.edu; mirica@illinois.edu; renske.vanderveen@helmholtz-berlin.de

Abstract

Photo-assisted catalysis using Ni complexes is an emerging field for cross-coupling reactions in organic synthesis. However, the mechanism by which light enables and enhances reactivity of these complexes often remains elusive. Although optical techniques have been widely used to study the ground and excited states of photocatalysts, they lack the specificity to interrogate the electronic and structural changes at specific atoms. Herein we report metal-specific studies using static and transient Ni L- and K-edge X-ray absorption spectroscopy of a prototypical Ni photocatalyst, (dtbbpy)Ni(*o*-tol)Cl (dtb = 4,4'-di-*tert*-butyl, *o*-tol = *ortho*-tolyl). We discovered that the ground state of this complex has a mixed-spin character of ~70/30% singlet/triplet. Furthermore, we confirm that the long-lived (~5 ns) excited state is a tetrahedral metal-centered triplet state. These results pave the way for the future design of Ni-bipyridine based photocatalysts by, for example, judiciously tuning the electronic and geometric properties of the ligands with the goal of increasing excited-state lifetimes and quantum yields of reactive species.

1. INTRODUCTION

Over the past several years, light-driven bond-forming reactions have become ubiquitous in synthetic organic chemistry[1–4]. Of particular interest is the merger of photochemistry with transition metal (TM) cross-coupling catalysis (e.g. photoredox catalysis), wherein a precious metal photosensitizer absorbs light and undergoes electron transfer with a TM catalyst, forming a highly reactive high-valent TM species that can unlock reactivity that is inaccessible in the ground state[5,6]. These photosensitizers can also undergo energy transfer to the TM complex, forming excited states via indirect light excitation pathways that have enhanced reactivity in comparison to the ground-state catalysts[6–8]. In some cases, the specific bond-forming process occurs with direct photoexcitation of the metal center and its tunable ligand system, eliminating the need for an exogenous, precious metal photosensitizer to absorb light[9–19]. These properties provide the opportunity to access previously elusive or unknown mechanistic pathways and enable the invention of a wide variety of nontraditional bond constructions in medicinal chemistry, natural product synthesis, and polymerization reactions[8,20–22].

To optimize the reactivity of photocatalysts, it is necessary to understand both their ground- and excited-state properties. X-ray absorption spectroscopy (XAS) is a powerful technique that can be implemented in any medium (gas phase, solution, solid) and provides an element-specific local probe of the electronic and geometric structures surrounding specific elements. XAS in the soft and hard X-ray ranges has been successfully used to reveal the ground- and excited-state properties of heterogeneous and homogeneous TM-based (photo)catalysts[23–45].

TM complexes based on earth-abundant Ni(II) and featuring the bidentate 2,2′-bipyridine (bpy) ligand have received significant attention in the field of photoredox and light-promoted catalysis in recent years[11,14,18,19,46,47]. The ground spin states and structures of Ni(II) d^8 complexes are highly dependent on the ligand field. Complexes with weak-field ligands typically adopt a tetrahedral or octahedral structure and a high-spin configuration while complexes with strong-field ligands favor a square-planar coordination and a low-spin configuration[48–50]. Exceptions to these rules have been reported. For example, the family of Ni[*t*-

$bu_2P(O)NR]_2$ complexes, where R = *i*Pr or *c*-hexyl, adopt square-planar geometries with S=1 spin states[51]. The ground-state spin and geometry of Ni(II) complexes have implications for their excited-state properties and reactivity, such as the ability to undergo triplet-triplet energy transfer[7].

In contrast to their second- and third-row transition metal counterparts, the ultrafast photophysics of Ni photocatalysts has only been scarcely studied, and the results of recent studies are often in conflict with one another[52–54]. The unambiguous determination of the nature and lifetime of excited states is crucial, as these states may be indirectly or directly responsible for the reaction outcome (i.e. product yield, selectivity, specificity, and byproducts). For example, the metal-to-ligand charge transfer (MLCT) state lifetime in second- and third-row transition metal d^6 complexes such as $Ru(bpy)_3$ is in the nanosecond (ns)-to-microsecond (μs) regime[55]. Such long-lived MLCT states leave sufficient time for bimolecular processes to occur in solution. In contrast, the MLCT excited states of first-row transition metals are generally deactivated rapidly (within tens of picoseconds (ps)) due to the presence of low-lying metal-centered d-d states[56]. In the case of Ni(bpy)-based photocatalysts, two mechanisms for light-promoted catalysis have been proposed. *Ab initio* calculations have suggested that reductive elimination from the triplet MLCT state directly leads to the formation of new C-heteroatom bonds[57,58]. Other experimental and theoretical work has proposed the population of ligand-to-metal charge transfer (LMCT)[54] or (d-d)[11,53] states, in which metal d-orbitals mix with antibonding ligand σ-orbitals, promoting metal-ligand bond cleavage and forming highly reactive intermediates (such as Ni(I) species) via a unimolecular process[17]. These reactive intermediates would then undergo a "dark" catalytic Ni(I)/Ni(III) cycle without the involvement of photons. However, there is no direct experimental evidence for any of these states or photocatalytic pathways, and their assignments heavily rely on *ab initio* calculations.

We present L- and K-edge XAS, supported by Evans method nuclear magnetic resonance (NMR) and superconducting quantum interference device (SQUID) magnetometry, of a characteristic Ni photocatalyst, (dtbbpy)Ni(*o*-tol)Cl (dtb = 4,4'-di-*tert*-butyl, *o*-tol = *ortho*-tolyl), which is the proposed ground-state analog to the intermediate species formed in the Ni photocatalytic cycle for carbon-heteroatom bond coupling

reactions[6,8,59]. We show that the ground state of (dtbbpy)Ni(*o*-tol)Cl exhibits a mixture of singlet and triplet character, rather than a pure singlet state as previously assumed[53]. The admixture of triplet character is expected to increase the relaxation rate for distorted triplet excited states back to the ground state by making the transition partially spin-allowed.

In addition to determining the ground-state properties of (dtbbpy)Ni(*o*-tol)Cl, we aimed to elucidate its excited-state dynamics upon light excitation. Previously, Doyle and co-workers reported that this complex exhibits an excited state that decays back to the ground state on the time scale of 3-8 ns, depending on the solvent[52,53]. They initially assigned this state to a long-lived MLCT state[52], which was later revised to be a tetrahedral ^{3}d-d state based on density functional theory (DFT) calculations[53]. While the latter study provides compelling evidence for the disappearance of the MLCT state within ~10 ps via time-resolved infrared (IR) spectroscopy, no direct experimental evidence is provided for the identity of this long-lived excited state. Optical spectra are congested and non-specific making unambiguous identification of metal-centered states difficult. X-ray absorption spectroscopy, on the other hand, offers a distinctive view since it is element-specific and directly sensitive to the metal-ligand interactions. In this work, we employ picosecond-resolved Ni L- and K-edge XAS to unambiguously determine the identity of the ~5 ns excited state in (dtbbpy)Ni(*o*-tol)Cl as a tetrahedral ^{3}d-d state. While ultrafast K-edge spectroscopy is well-established for Ni coordination compounds[39,40,60,61], the Ni L-edge has been completely unexplored so far in this time regime.

The determination of ground- and excited-state properties using X-ray spectroscopy and magnetometry in this work has profound implications for the future development of Ni(II) photocatalysts where careful synthetic ligand design may enable tuning of excited-state lifetimes, reaction pathways, and quantum yields.

2. RESULTS AND DISCUSSION

2.1 Ground-State Characterization

2.1.1. L-edge X-ray Absorption Spectroscopy. In first-row TM complexes, soft X-ray $L_{3,2}$-edge spectroscopy locally probes the empty 3d density of states at the metal center through dipole-allowed 2p→3d transitions and is thereby sensitive to metal-ligand covalency, the metal oxidation state, spin state, and local coordination symmetry[32,62–66]. We performed solution-phase Ni L-edge spectroscopy in transmission mode to characterize the ground state of (dtbbpy)Ni(*o*-tol)Cl in dimethylformamide (DMF) (see Supporting Information (SI) Section S1 for synthetic details). The Ni $L_{2,3}$-edge transitions lie at approximately 850 eV ($2p_{3/2}$-core excitation, L_3 edge) and 870 eV ($2p_{1/2}$-core excitation, L_2 edge). Because soft X-rays at these energies are heavily absorbed and scattered by matter, a very thin liquid sheet of sample must be formed in a vacuum chamber. For this purpose, we used a vacuum-compatible colliding liquid jet with a sheet thickness of approximately 2 μm as part of the *nmTransmissionNEXAFS* end station at beamline UE52_SGM of the BESSY II synchrotron facility[67,68] (see SI Section S2 for more details).

Fig. 1 shows the ground-state $L_{2,3}$-edge spectra of 20 mM (dtbbpy)Ni(*o*-tol)Cl in DMF, together with several simulated spectra using the CTM4XAS code[69]. The energy was calibrated based on spectra reported in the literature[70]. The L_3-edge spectrum contains one main peak (A) at 853.4 eV, with a prominent shoulder (A') on the red side at approximately 852.6 eV and a weaker shoulder (A_2) on the blue side at approximately 854.6 eV. The L_2-edge spectrum features one main peak; the lower energy shoulder visible in the simulation could not be clearly resolved.

Based on the literature[52,53], we expected the (dtbbpy)Ni(*o*-tol)Cl complex to adopt a square-planar low-spin structure. Previous work on four-coordinate low-spin Ni complexes such as porphyrins and phthalocyanines shows a strong, sharp L_3-edge absorption feature at ~854 eV assigned to the $2p_{3/2} \rightarrow 3d_{x^2-y^2}$ transition and a well-separated feature about 1.5 eV higher in energy assigned to transitions from $2p_{3/2}$ to hybridized Ni 3d–N 2p orbitals[71]. Single, sharp $2p_{3/2} \rightarrow 3d_{x^2-y^2}$ absorption features are observed for

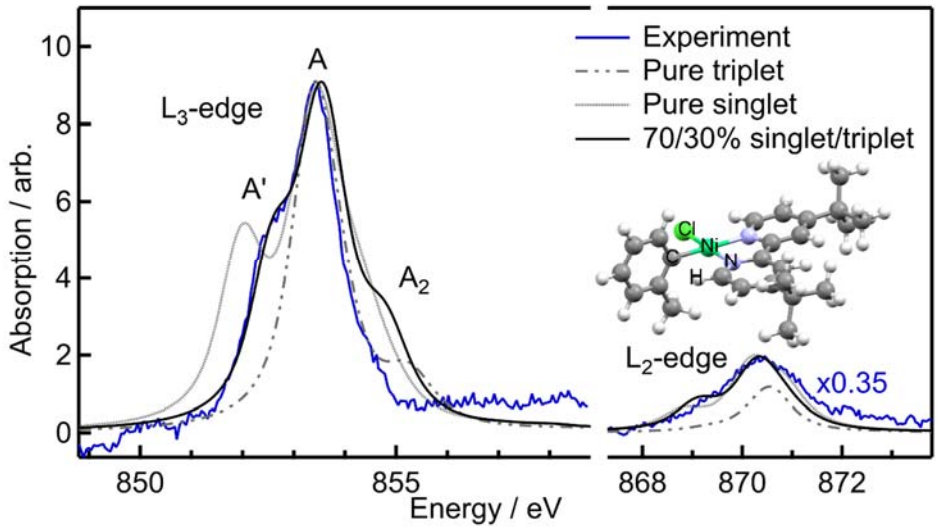

Figure 1. Experimental L_3- and L_2-edge XAS spectra (blue trace) with simulated spectra featuring different ratios between singlet and triplet character in gray and black. The simulated spectra are arbitrarily scaled to match the intensity of the L_3-edge white line, and the L_2-edge experimental data is arbitrarily scaled to match the intensity of the resulting simulated L_2-edge peak for a mixture of 70/30% singlet/triplet character.

bioinorganic low-spin Ni(II) complexes such as [NiFe] hydrogenases as well as model complexes such as NiF_2 and Ni[bis(diphenylbis((methylthio)methyl)borate)][70]. This single peak splits into two peaks for high-spin Ni(II), nominally because there are now two d holes (d_{z^2} and $3d_{x^2-y^2}$) available for the $2p_{3/2} \rightarrow 3d$ transition[70]. The presence of the high-energy shoulder (A_2) alone is thus not a good indicator of either a low- or high-spin configuration in Ni(II) complexes. We therefore focus on the low-energy shoulder (A').

The low-energy shoulder (A') observed in the L_3-edge spectrum is atypical for low-spin Ni(II). In order to better understand this feature, we performed semiempirical ligand-field multiplet simulations using the CTM4XAS software package[69,72] (see SI Section S2.1 for details). This method uses a parametric Hamiltonian that represents the crystal field strength and symmetry, describing the ground state as a linear combination of crystal field configurations such as $\Psi = \alpha_1 d_{\pi}^4 d_{xy}^2 d_{z2}^2 d_{x2-y2}^0 + \alpha_2 d_{\pi}^4 d_{xy}^2 d_{z2}^1 d_{x2-y2}^1 + \cdots$, where the energy of each configuration is given by the crystal field parameters 10Dq, Ds, and Dt for a system with D_{4h} symmetry. In systems with appreciable covalency, additional configurations accounting for charge transfer to/from a ligand are added and parametrized by the energy difference and coupling strength between the $d^N L$ and $d^{N+1}L^+$ states. These configurations are mixed via spin-orbit coupling resulting

in a manifold of electronic states. Transition dipole matrix elements are then calculated between the $3d^N$ ground state and $2p^5 3d^{N+1}$ excited states to produce an XAS spectrum.

Beginning with ligand-field parameters developed for low-spin Ni(II)octaethylporphyrin[73], we adjusted the ligand field until we reproduced the low-energy shoulder. The best match between simulation and experiment is shown in Fig. 1. The energy spacing between the main peak A and the low-energy shoulder A' as well as their intensity ratio show an excellent match to the experiment, though the strength of the high-energy shoulder A_2 is overestimated in the simulation of the L_3-edge spectrum. Inspection of the ground state generated by this ligand field reveals a quantum mixture of approximately 70% singlet and 30% triplet character. Small changes to the ligand-field parameters (±0.05 eV) also gave reasonable matches to experiment, and the resulting ground states have triplet character ranging from 30% to 50% (Fig. S2A). We were unable to reproduce the experimental low-energy shoulder A' using any ligand field that produces a pure-singlet ground state. Although the semiempirical nature of this calculation (which for example does not account for the true C_1 symmetry of the molecule) does not allow a quantitative measure of the actual triplet character, this analysis indicates that (dtbbpy)Ni(*o*-tol)Cl cannot be described simply as a singlet ground state. As shown in Fig. S2B, a reasonable correspondence to the experimental spectrum can also be obtained for a linear combination of pure-singlet and pure-triplet simulated spectra. Thus, the L-edge spectrum alone is not sufficient to determine whether we have a quantum admixture of singlet and triplet or a statistical mixture of the two. Below in Section 2.1.3 we confirm the former scenario with SQUID magnetometry.

We note that the $L_{3,2}$ spectrum of (dtbbpy)Ni(*o*-tol)Cl in powder form is nearly identical to the solution-phase spectrum (Fig. S1). Since the crystal structure shows a nearly square-planar geometry around the Ni center[52], this rules out the possibility of solvent coordination and significant distortions away from square-planar symmetry in solution. Paramagnetic square-planar ground states have previously been observed in sterically hindered Ni(II) coordination compounds[74]. Here we report this admixture of singlet/triplet spin state character for the first time for a prototypical Ni(II)-bipyridine organometallic photocatalyst.

2.1.2. Nuclear Magnetic Resonance. Based on these intriguing results, we decided to investigate the ground-state spin character using Evans method NMR (see SI Section S3 for details). This technique enables the determination of the magnetic susceptibility in cases of paramagnetic samples[75,76]. The NMR experiments were performed in deuterated solvents and with an internal standard for calibration of the peak integrals. They were performed in DMF, dichloromethane (DCM), and tetrahydrofuran (THF) at varying concentrations. All solvents and concentrations yield the same results. Variable-temperature Evans method NMR was performed on the complex in DCM.

NMR measurements of the complex without an added internal standard exhibit sharp, diamagnetic peaks that integrate to the expected values. However, adding an internal standard (benzodioxole) to the NMR tube and spin integrating with respect to the standard peaks reveals a significantly decreased integration of the peaks corresponding to the diamagnetic, singlet-state complex, suggesting that the complex may contain only ~45% of diamagnetic material (Fig. S5). We therefore carried out Evans method NMR measurements in which a capillary containing deuterated solvent and benzodioxole is placed inside an NMR tube containing (dtbbpy)Ni(*o*-tol)Cl and benzodioxole, and the shift in the benzodioxole peaks is quantified. The Evans method yields a μ_{eff} of 1.76 Bohr Magnetons (μ_B) at room temperature, which is an intermediate value between the pure singlet value (μ=0 μ_B) and the value of $\mu \sim 4\ \mu_B$ expected for a four-coordinate triplet Ni(II) complex[77,78]. While this could indicate an S=½ system (μ=1.73), we are confident

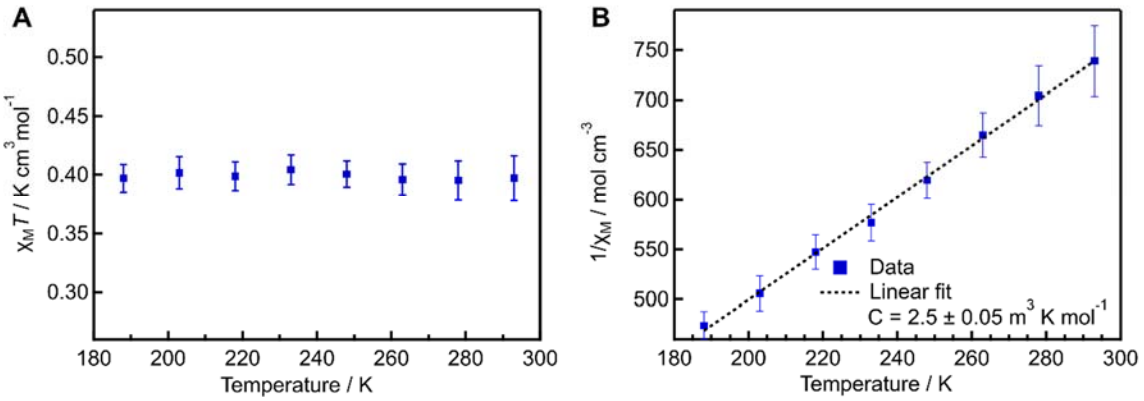

Figure 2. (A) Temperature dependence of $\chi_M T$ determined from variable-temperature Evans method NMR on 10mM (dtbbpy)Ni(*o*-tol)Cl in d2-DCM. (B) Linear dependence of $1/\chi_M$ vs. T indicating that the Curie-Weiss law applies. The slope corresponds to the Curie constant, C.

that the complex has a d^8 electron configuration based on the similarity of K-edge XAS experiments with previous spectra of Ni d^8 compounds (Section S6). The possibility of solvent binding to the Ni(II) center causing a change to a triplet ground state was further ruled out by measurements in non-coordinating solvents (DCM), which yield the same μ_{eff} values as in coordinating solvents (DMF or THF) (Table S2), as well as by solid-state magnetometry experiments described below. The possibility of aggregation was ruled out by Evans method NMR measurements in d2-DCM across a broad range of concentrations, and no dependence of μ_B on the concentration of sample is observed (Fig. S8)[79].

To further investigate the paramagnetic character of the ground-state complex, we performed variable-temperature Evans method NMR experiments. Plotting $\chi_M T$ versus temperature (T) yields a relatively flat line with a value of approximately 0.4 cm^3 K mol^{-1} after the diamagnetic correction (Fig. 2A). This shows that the paramagnetic susceptibility is fairly constant in the temperature range of the experiment, which is characteristic of paramagnetic species[80]. Plotting $1/\chi_M$ versus T yields a linear plot, which indicates that the complex is following the Curie-Weiss law for paramagnetic materials (Fig. 2B). The slope corresponds to the Curie constant and is fitted to a value of 2.5 ± 0.05 m^3 K mol^{-1}. These results corroborate the findings from the L-edge data and confirms that the complex contains high-spin character.

2.1.3. SQUID Magnetometry. SQUID magnetometry measurements were carried out on the solid sample at a constant dc field of 1000 Oe between 300 K and 2 K (Fig. 3) (see SI Section S4 for details). Paramagnetic materials feature positive susceptibilities with a strong increase in susceptibility at low temperature where magnetic interactions prevail over thermal fluctuations. The measured room temperature $\chi_M T$ is 0.43 cm^3 K mol^{-1}, in good agreement with the NMR results (Fig. 2A). A linear $1/\chi_M$ versus T dependence is obtained in the temperature range 2 K – 300 K (Fig. 3B). The slope yields a Curie constant of 2.80 ± 0.05 m^3 K mol^{-1}, which is in good agreement with the value determined from the variable-temperature Evans method NMR data (Fig. 2B).

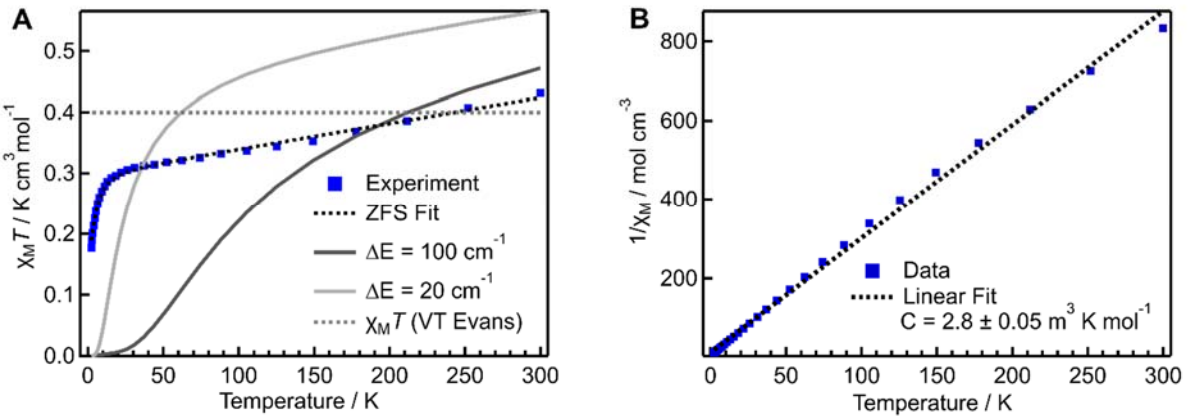

Figure 3. (A) $\chi_M T$ vs T of (dtbbpy)Ni(o-tol)Cl in the solid state from SQUID magnetometry (blue squares) with a fit to the zero-field splitting (ZFS) model (black dashed line, g = 2, D-value = -12 ± 0.5 cm^{-1}, temperature-independent paramagnetism = 0.00042 ± 0.00001, triplet-state fraction = 30%), which is a model of a quantum-mechanical mixture of singlet and triplet states. Simulated data sets using the ZFS model assuming a Boltzmann distribution of singlet and triplet states with energy splitting between the singlet and triplet states of 20 cm^{-1} and 100 cm^{-1} between the triplet and singlet states (statistical mixtures, light and dark gray solid lines, respectively). The gray dashed line denotes the experimentally determined $\chi_M T$ value determined from variable-temperature (VT) Evans method. (B) Linear dependence of $1/\chi_M$ vs T from the SQUID magnetometry experiment. The slope of the linear fit is the Curie constant, C.

As discussed in Section 2.1.1 and Section S2, both a quantum-mechanical admixture and a linear combination of singlet and triplet spectra adequately reproduce the ground-state L-edge spectra. Therefore, we simulated the magnetometry $\chi_M T$ *vs* T data using the zero-field splitting (ZFS) model with a temperature-independent percentage of triplet character (*i.e*, a quantum admixture), or with a Boltzmann distribution of singlet and triplet states (*i.e*, a statistical mixture, see SI Section S4 for details)[81]. The Boltzmann distribution clearly fails to adequately model the data, even for small (~20 cm^{-1}) energy differences between singlet and triplet states (Fig. 3A). However, the ZFS model using the temperature-independent quantum mixture of singlet/triplet states fits the data very well. In this model, the g-factor and triplet-state fraction are highly correlated fitting parameters. For reasonable values of the g-factor between 1.9 and 2.2[80,82], the triplet-state fraction is fitted to 25-33% (Fig. S10), in good agreement with the values determined from L-edge X-ray spectroscopy (~30%, Section 2.1.1) and Evans method NMR (~45%, Section 2.1.2). The D-value is fitted to -12 ± 0.5 cm^{-1}, and the temperature-independent paramagnetism is fitted to 0.00042 ± 0.00001 cm^3 mol^{-1}; both are reasonable values compared to those reported in the literature[51,82].

We thus conclude that the (dtbbpy)Ni(*o*-tol)Cl complex exhibits a quantum mechanically mixed-spin ground state, instead of a pure singlet ground state as previously assumed[52–54]. Such spin-state mixtures have been previously observed in heme systems[83], but to our knowledge this is the first report of such a quantum mixed-spin state in a Ni(II) organometallic complex.

2.2 Nature of the Long-Lived Excited State

Armed with new knowledge on the ground-state properties of (dtbbpy)Ni(*o*-tol)Cl, we aimed to determine the identity of the long-lived photoinduced excited state using X-ray transient absorption (XTA) spectroscopy. Previous optical and IR transient absorption experiments were done with excitation at >400 nm, and showed features of vibrational cooling in the MLCT manifold on the ~1 ps timescale, decay into a metal-centered triplet state on the 5-10 ps timescale, and back-relaxation to the ground state on the few ns timescale[53]. In the L-edge XTA experiments reported here (Section 2.2.1), the pump wavelength was chosen to be 343 nm overlapping with the red edge of the ligand $\pi \rightarrow \pi^*$ transition (Fig. S11). Our optical transient absorption (OTA) data (SI Section S5.1) show that for this excitation wavelength, the MLCT states are populated promptly, and the consequent dynamics is similar as for longer excitation wavelengths. We conclude that in our XTA experiments at ~100 ps time delay, the same long-lived state with a lifetime of ~ 5 ns is populated as in previous studies with lower-energy excitation[52,53].

2.2.1. Transient L-edge XAS. We performed laser pump – soft X-ray probe experiments at the UE52-SGM beam line at BESSY II[67] on a 20 mM solution of (dtbbpy)Ni(*o*-tol)Cl in DMF (see SI Section S4 for experimental details). The transient (laser on minus laser off) Ni $L_{3,2}$-edge spectra at ~100 ps time delay (343 nm, 350 fs pump, 208 kHz, 3 mJ/cm^2 absorbed fluence) are shown in Fig. 4A, together with the ground-state spectra for comparison. On first sight, both edges seem to shift to lower energy upon photoexcitation, which may be due to changes in charge density at the Ni center[84–86] or changes in ligand-field strength and/or symmetry[70,87]. Kinetic monitoring at 852 eV, corresponding to the peak of the L_3-edge

transient, yields a single-exponential decay with a decay time of 4890 ps ± 230 ps, in excellent agreement with the ground-state recovery time determined in OTA experiments (Fig. S14). This confirms that we are probing the longest-lived excited state of (dtbbpy)Ni(*o*-tol)Cl whose nature we seek to unambiguously determine here.

To this extent, we investigated several excited-state scenarios using the ligand-field multiplet method described in Section 2.1.1 (details are provided in SI Section S2.1). First, we calculated the spectra for Ni with d^7 and d^9 electron configurations, instead of d^8 for Ni(II), in order to qualitatively simulate square-

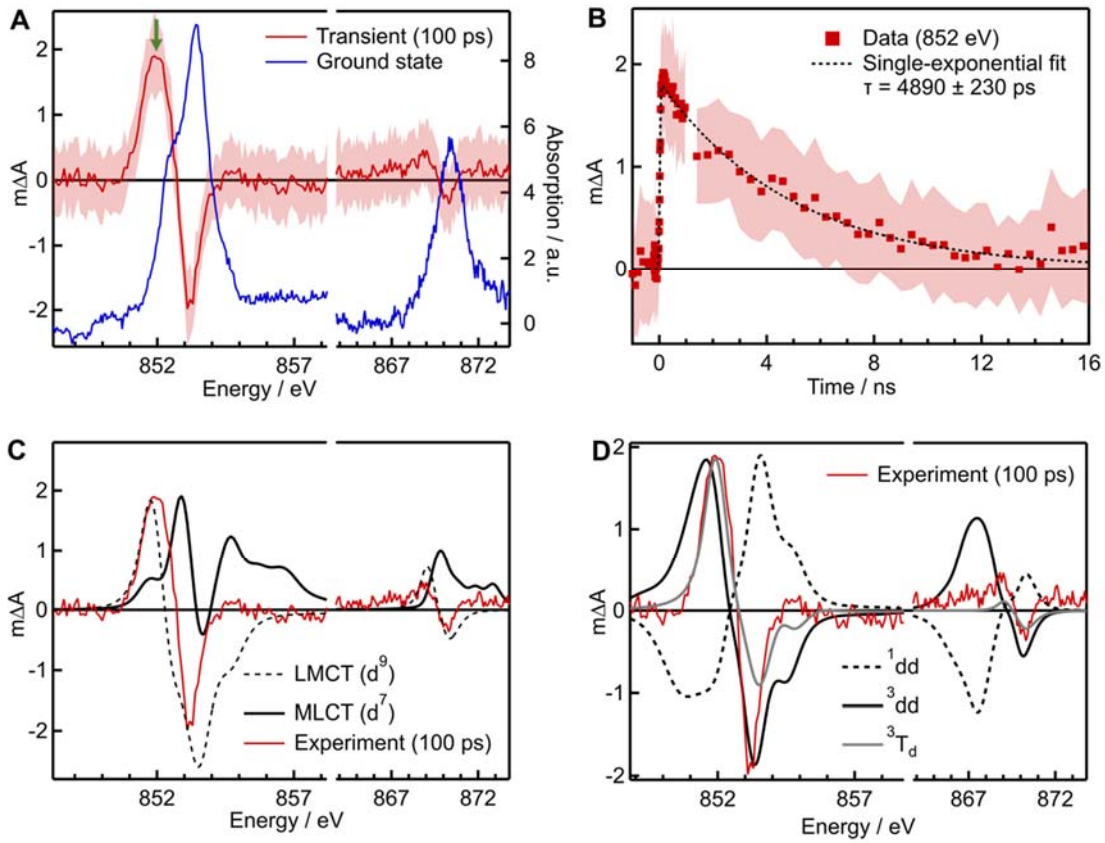

Figure 4. (A) L_3-edge transient spectrum of 20 mM (dtbbpy)Ni(*o*-tol)Cl in DMF at ~100 ps after photoexcitation at 343 nm (red) together with the ground-state spectrum in blue; (B) Kinetic trace collected at 852 eV (peak of the L_3 transient, green arrow in panel A) with the single-exponential fit shown in the dashed line; (C) Simulated difference spectra using d^7 (solid black, "MLCT state") and d^9 (dashed black, "LMCT state") electron configurations for Ni, together with the experimental transient spectrum (red; same as in A); (D) Simulated difference spectra using high-lying ^{3}d-d (solid black) and ^{1}d-d (dashed black) states with the square-planar ground-state ligand field symmetry and parameters. The simulated difference spectrum using a tetrahedral ligand field is shown in gray. The experimental transient spectrum (red) is added for comparison (same as in A). Shaded areas in A and B denote standard error. The simulated spectra in C and D have been arbitrarily scaled to match the intensity of the experimental data at 853.4 eV.

planar excited states with MLCT or LMCT character (Fig. 4C). All simulations were performed with the same ligand-field and charge-transfer parameters as the best-match simulation for the ground state (Fig. 1); however, the d^9 state did not include charge transfer, as the addition of charge transfer would invoke a d^{10} state, which has no $L_{3,2}$-edge intensity. The simulated ground-state spectrum was subtracted to generate difference spectra to compare to the experimental transient spectrum at ~100 ps after photoexcitation. Overall, the spectra of states with different d-electron counts do a poor job of simulating the experimental data. Although the d^9 ("LMCT") state features a red shift, the simulated spectrum is much broader than the experimental spectrum.

Next, d^8 square-planar excited states were considered (d-d states) (Fig. 4D). The simulated difference spectrum for a square-planar excited ^{1}(d-d) state features a blue shift, which is the opposite of what is seen in the experiment. On the other hand, the simulated difference spectrum for a square-planar excited ^{3}(d-d) state exhibits a reasonable match at the L_3 edge, but the width of the transient features and the red shift at the L_2-edge are heavily overestimated. Finally, we considered a geometric change in the excited state. DFT calculations indicate that the lowest-lying triplet state has tetrahedral geometry[53], and so we simulated a triplet state with a tetrahedral ligand field without charge transfer character (Fig. 4D). This excited-state simulation exhibits the best match to the experiment at both edges in terms of peak position and width of the transient features. The discrepancy in bleach intensity at the L_3-edge between the experiment and the simulation may be due to the assumption that the CTM4XAS program requires the selection of a specific geometry and cannot account for the true C_1 symmetry of the complex, nor for any geometries deviating from pure point-group symmetries (e.g. slight distortions away from square-planar geometry as suggested by the crystal structure of (dtbbpy)Ni(*o*-tol)Cl)[52]). Our L-edge XTA data thus strongly supports the assignment of the long-lived excited state of (dtbbpy)Ni(*o*-tol)Cl as the tetrahedral metal-centered ^{3}(d-d) state predicted by DFT (SI Section S7), in agreement with the proposed state assignment by Doyle *et al*[11,17,53,61,88].

2.2.2. Transient K-edge XAS. We performed static and transient XAS measurements of the (dtbbpy)Ni(*o*-tol)Cl complex (5 mM in DMF) at the Ni K-edge at beam line 11-ID-D of the Advanced Photon Source (APS)[89] (see SI Section S6 for experimental details). K-edge spectra of first-row TM complexes involve the excitation of a 1s electron to empty 4p states and are highly sensitive to local geometry about the metal center[90]. The K-edge data are shown in Fig. 5. The static spectrum (Fig. 5A) features a shoulder at the low-energy side of the white line at 8337.5 eV, which is assigned to the 1s→4p_z transition[39,91]. The Ni 4$p_{x,y}$ orbitals are higher in energy than the 4p_z orbitals in square-planar complexes due to strong σ-interactions between the 4$p_{x,y}$ orbitals and the ligand 2s orbitals[61]

The transient K-edge spectrum recorded at ~100 ps after photoexcitation (515 nm, 20 mJ/cm^2 absorbed fluence, 120 fs) is shown in Fig. 5A. The kinetics were monitored at 8337.5 eV corresponding to the peak of the 4p_z bleach (Fig. 5B). A single-exponential decay with a time constant of 5310 ps ± 530 ps is obtained, in good agreement with both the time-resolved optical (Section S5) and L-edge data (Fig. 4B). The transient spectrum exhibits a bleaching of the 1s → 4p_z rising-edge feature and an increase in intensity at the white line (1s → 4$p_{x,y}$) (Fig. 5A). This suggests that in the excited state, the 1s→4p_z absorption band shifts to higher energies due to destabilization of the 4p_z orbital. The latter is consistent with the geometric

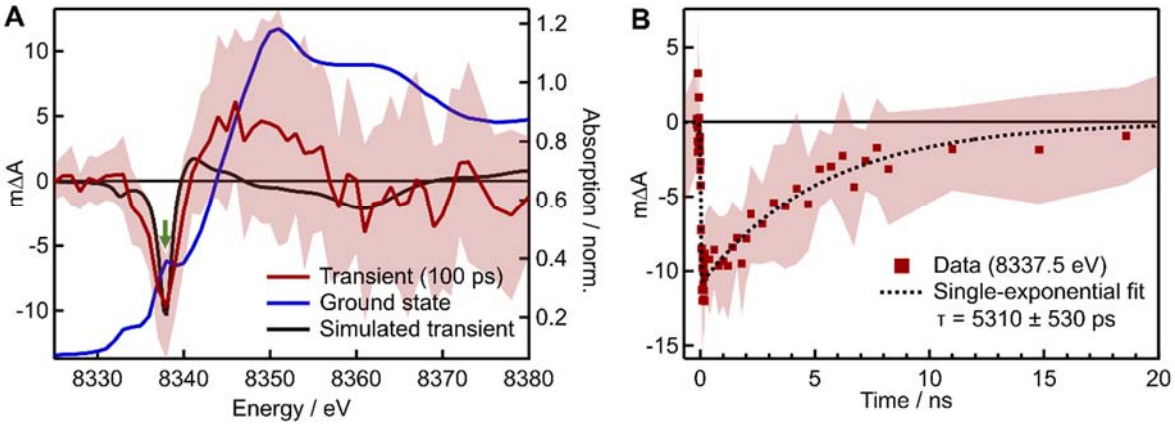

Figure 5. (A) Ground-state K-edge spectrum in blue with pump-probe signal measured at a 100 ps delay in red and simulated transient spectrum in black. The latter has been scaled by a factor of 0.01 to match the amplitude of the bleach feature at 8337.5 eV. (B) Kinetic monitoring at 8337.5 eV (green arrow in panel A) showing a decay time of 5310 ± 530 ps, in good agreement with optical and L-edge measurements. Shaded areas denote standard error.

reorganization to a T_d ligand field in the ^{3}d-d excited state, in which all Ni 4p orbitals are hybridized with 3d orbitals and degenerate.

To corroborate this interpretation, we performed simulations of the Ni K-edge spectrum using the real-space, full-potential FDMNES code.[92,93] The simulated difference spectrum is generated by subtracting the normalized ground-state simulation from the normalized excited-state simulation using the geometry-optimized square-planar and tetrahedral geometries from DFT as input structures, respectively (SI Section S7). The resulting (scaled) difference spectrum shows a reasonable match to the experimental transient spectrum, with a decrease in intensity at the 1s → $4p_z$ peak and a slight increase in intensity in the white line region (Fig. 5A). The simulated transient is scaled by a factor of 0.01 to match the intensity of the ground-state bleach, which indicates an excitation fraction of ~1%. However, this factor is artificially low due to the overestimated strength of the 1s → $4p_z$ transition in the ground-state simulation by approximately a factor of 10 (Fig. S16). The excitation fraction is therefore actually closer to ~10%. In Section S6 we show that the intensity of the 1s → $4p_z$ peak is particularly sensitive to the dihedral angle between the bipyridine plane and the (*o*-tol)Cl plane; the larger the angle, the lower the intensity of the pre-edge peak. The intensity of the transient 1s → $4p_z$ bleach feature is thus a unique signature of a structural distortion away from the square-planar ground-state geometry.

Qualitatively, these observations are similar to the transient K-edge spectra observed for Ni(II) porphyrins or Ni(II) phthalocyanines in coordinating solvents[39,40,60,94]. The long-lived transient states in coordinating solvents of Ni(II) porphyrins and phthalocyanines involve solvent coordination to the Ni(II) center to form an octahedral complex from a square-planar ground state, destabilizing the $4p_z$ orbital as evidenced sensitively in the pre-edge region of the K-edge spectrum.

3. Conclusion

Using a combination of static $L_{2,3}$-edge X-ray spectroscopy and magnetometry we found that the ground state of (dtbbpy)Ni(*o*-tol)Cl exhibits a nearly square-planar geometry with a quantum mixture of ~70/30% singlet/triplet character, as opposed to the pure singlet character as previously assumed. This finding represents an interesting exception to the common assumption that Ni(II) complexes either adopt a tetrahedral high-spin structure with weak-field ligands, or a square-planar low-spin structure with strong-field ligands[48–50]. We believe that the quantum mixture of singlet and triplet character observed for (dtbbpy)Ni(*o*-tol)Cl is a consequence of the fact that the complex is in an intermediate ligand-field regime, namely containing one weak-field ligand (Cl) and one strong-field ligand (*o*-tol). Furthermore, steric interactions between the *ortho*-tolyl and bipyridine ligands may play a role as well. Such steric effects have been inferred in paramagnetic Ni(II) ground-state complexes[74], as well as mixed-spin heme systems[83]. Using transient L-edge and K-edge X-ray spectroscopy, we unambiguously determined that the lowest excited state of (dtbbpy)Ni(*o*-tol)Cl is a tetrahedral triplet ^{3}(d-d) state with a life time of ~5 ns for back-relaxation to the ground state. The triplet admixture in the ground state thus shortens the lifetime by making the back-relaxation from the ^{3}(d-d) state partially spin-allowed. Hence, these results open the possibility of prolonging the excited-state life time of (dtbbpy)Ni(*o*-tol)Cl by reducing the contribution of triplet character in the ground state. Future X-ray spectroscopy and magnetometry studies with different ligands, systematically tuning both ligand field and sterics, will provide synthetic handles to disentangle the factors leading to quantum mixed ground states in Ni(II) complexes.

TOC Graphic

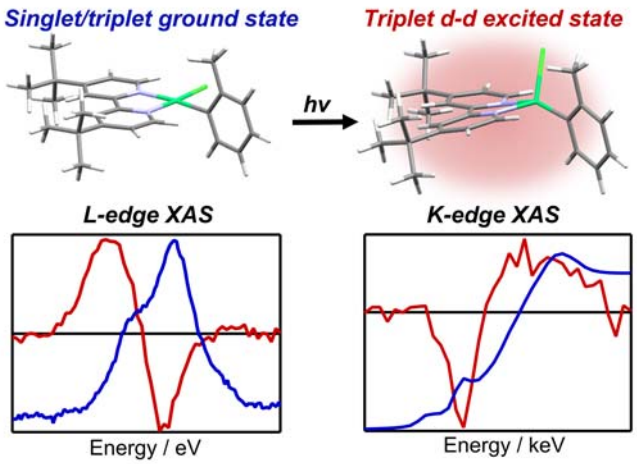

ASSOCIATED CONTENT

Supporting Information

Synthetic details, UV/visible absorption spectroscopy and TDDFT spectra, optical transient absorption spectroscopy and related fits, L-edge experimental details, K-edge experimental details, ^{1}H NMR spectra, magnetometry experimental details, and simulation details. This material is available free of charge via Internet at http://pubs.acs.org.

AUTHOR INFORMATION

Corresponding authors

Liviu Mirica – mirica@illinois.edu

Josh Vura-Weis – vuraweis@illinois.edu

Renske van der Veen – renske.vanderveen@helmholtz-berlin.de

ORCID

Rachel Wallick - 0000-0002-7548-4850

Sagnik Chakrabarti - 0000-0002-0757-1127

John Burke - 0000-0001-9853-7292

Richard Gnewkow - 0000-0002-6524-4909

Ju Byeong Chae - 0000-0001-7558-5814

Thomas Rossi- 0000-0002-7448-8948

Ioanna Mantouvalou – 0000-0002-9696-2970

Birgit Kanngießer - 0000-0001-6508-0150

Mattis Fondell - 0000-0003-2689-8878

Sebastian Eckert - 0000-0002-1310-0735

Conner Dykstra - 0000-0001-5597-6914

Laura Smith - 0000-0002-7890-497X

Liviu Mirica- 0000-0003-0584-9508

Josh Vura-Weis - 0000-0001-7734-3130

Renske van der Veen - 0000-0003-0584-4045

Acknowledgements

The authors acknowledge the use of facilities and instrumentation at the Materials Research Laboratory Central Research Facilities, University of Illinois, partially supported by NSF through the University of Illinois Materials Research Science and Engineering Center DMR-1720633. This work was supported by a Packard Fellowship in Science and Engineering from the David and Lucile Packard Foundation (RMvdV, RFW) and by NSF CHE-2155160 (LMM, SC, JBC). JHB acknowledges support by the National Science Foundation Graduate Research Fellowship Program under Grant No. DGE21-46756 and the Robert C. and Carolyn J. Springborn Endowment for Student Support Program. This material is based upon work supported by the U.S. Department of Energy, Office of Science, Office of Basic Energy Sciences under Awards Number DE-SC0018904 (JVW, LMM, RFW) and DE-SC0021062 (CD). Solid-

state NEXAFS spectroscopy was carried out with the support of Diamond Light Source, beamline B07-C (proposal cm31118-3). The authors acknowledge assistance from Frank de Groot and Matthijs Van Spronsen with this measurement. Solution-phase L-edge measurements were carried out at the UE52_SGM beamline, nmTransmission NEXAFS end station at the BESSY II electron storage ring operated by the Helmholtz-Zentrum Berlin für Materialien und Energie GmbH. We would like to thank Robby Büchner for assistance during the experiment. This research used resources of the Advanced Photon Source, a U.S. Department of Energy (DOE) Office of Science user facility operated for the DOE Office of Science by Argonne National Laboratory under Contract No. DE-AC02-06CH11357. We would like to thank Xiaoyi Zhang, Rick Spence, Burak Guzelturk, and Jin Yu for assistance during the experiment.

References

(1) Remy, R.; Bochet, C. G. Arene-Alkene Cycloaddition. *Chem. Rev.* **2016**, *116* (17), 9816–9849.

(2) Poplata, S.; Tröster, A.; Zou, Y. Q.; Bach, T. Recent Advances in the Synthesis of Cyclobutanes by Olefin [2 +2] Photocycloaddition Reactions. *Chem. Rev.* **2016**, *116* (17), 9748–9815.

(3) Ghogare, A. A.; Greer, A. Using Singlet Oxygen to Synthesize Natural Products and Drugs. *Chem. Rev.* **2016**, *116* (17), 9994–10034.

(4) Ravelli, D.; Protti, S.; Fagnoni, M. Carbon-Carbon Bond Forming Reactions via Photogenerated Intermediates. *Chem. Rev.* **2016**, *116* (17), 9850–9913.

(5) Chan, A. Y.; Perry, I. B.; Bissonnette, N. B.; Buksh, B. F.; Edwards, G. A.; Frye, L. I.; Garry, O. L.; Lavagnino, M. N.; Li, B. X.; Liang, Y.; Mao, E.; Millet, A.; Oakley, J. V.; Reed, N. L.; Sakai, H. A.; Seath, C. P.; MacMillan, D. W. C. Metallaphotoredox: The Merger of Photoredox and Transition Metal Catalysis. *Chem. Rev.* **2022**, *122* (2), 1485–1542.

(6) Twilton, J.; Le, C. C.; Zhang, P.; Shaw, M. H.; Evans, R. W.; MacMillan, D. W. C. The Merger of Transition Metal and Photocatalysis. *Nat. Rev. Chem.* **2017**, *1*.

(7) Welin, E. R.; Le, C.; Arias-Rotondo, D. M.; McCusker, J. K.; MacMillan, D. W. C. Photosensitized, Energy Transfer-Mediated Organometallic Catalysis through Electronically Excited Nickel(II). *Science* **2017**, *355* (6323), 380–385.

(8) Terrett, J. A.; Cuthbertson, J. D.; Shurtleff, V. W.; MacMillan, D. W. C. Switching on Elusive Organometallic Mechanisms with Photoredox Catalysis. *Nature* **2015**, *524* (7565), 330–334.

(9) Shen, X.; Li, Y.; Wen, Z.; Cao, S.; Hou, X.; Gong, L. A Chiral Nickel DBFOX Complex as a Bifunctional Catalyst for Visible-Light-Promoted Asymmetric Photoredox Reactions. *Chem. Sci.* **2018**, *9* (20), 4562–4568.

(10) Lim, C. H.; Kudisch, M.; Liu, B.; Miyake, G. M. C-N Cross-Coupling via Photoexcitation of Nickel-Amine Complexes. *J. Am. Chem. Soc.* **2018**, *140* (24), 7667–7673.

(11) Cavedon, A. C.; Gisbertz, S.; Reischauer, S.; Schrottke, S.; Hsu, W.; Anghileri, L. Intraligand Charge Transfer Enables Visible-Light-Mediated Nickel-Catalyzed Cross-Coupling Reactions. *Angew. Chemie Int. Ed.* **2022**.

(12) Sun, R.; Qin, Y.; Ruccolo, S.; Schnedermann, C.; Costentin, C.; Nocera, D. G. Elucidation of a Redox-Mediated Reaction Cycle for Nickel-Catalyzed Cross Coupling. *J. Am. Chem. Soc.* **2019**, *141* (1), 89–93.

(13) Sun, R.; Qin, Y.; Nocera, D. G. General Paradigm in Photoredox Nickel-Catalyzed Cross-Coupling Allows for Light-Free Access to Reactivity. *Angew. Chemie - Int. Ed.* **2020**, *59* (24), 9527–9533.

(14) Yang, L.; Lu, H. H.; Lai, C. H.; Li, G.; Zhang, W.; Cao, R.; Liu, F.; Wang, C.; Xiao, J.; Xue, D. Light-Promoted Nickel Catalysis: Etherification of Aryl Electrophiles with Alcohols Catalyzed by a NiII-Aryl Complex. *Angew. Chemie - Int. Ed.* **2020**, *59* (31), 12714–12719.

(15) Na, H.; Watson, M. B.; Tang, F.; Rath, N.; Mirica, L. M. Photoreductive Chlorine Elimination from a Ni(III)Cl 2 Complex Supported by a Tetradentate Pyridinophane Ligand . *Chem. Commun.* **2021**, *2076279*, 1–4.

(16) Song, G.; Yang, L.; Li, J. S.; Tang, W. J.; Zhang, W.; Cao, R.; Wang, C.; Xiao, J.; Xue, D. Chiral Arylated Amines via C−N Coupling of Chiral Amines with Aryl Bromides Promoted by Light. *Angew. Chemie - Int. Ed.* **2021**, *60* (39), 21536–21542.

(17) Na, H.; Mirica, L. M. Deciphering the Mechanism of the Ni-Photocatalyzed C–O Cross-Coupling Reaction Using a Tridentate Pyridinophane Ligand. *Nat. Commun.* **2022**, *13* (1), 1–11.

(18) Li, R.; Yang, C. X.; Niu, B. H.; Li, L. J.; Ma, J. M.; Li, Z. L.; Jiang, H.; Cheng, W. M. Visible

Light-Induced Ni-Catalyzed C-Heteroatom Cross-Coupling of Aryl Halides via LMCT with DBU to Access a Ni(i)/Ni(Iii) Cycle. *Org. Chem. Front.* **2022**, *9* (14), 3847–3853.

(19) Song, G.; Nong, D. Z.; Li, J. S.; Li, G.; Zhang, W.; Cao, R.; Wang, C.; Xiao, J.; Xue, D. General Method for the Amination of Aryl Halides with Primary and Secondary Alkyl Amines via Nickel Photocatalysis. *J. Org. Chem.* **2022**, *87* (15), 10285–10297.

(20) Brecht, R.; Frank Büttner; Böhm, M.; Seitz, G.; Frenzen, G.; Pilz, A.; Massa, W. Photooxygenation of the Helimers of (-)-Isocolchicine: Regio- and Facial Selectivity of the [4 + 2] Cycloaddition with Singlet Oxygen and Surprising Endoperoxide Transformations. *J. Org. Chem.* **2001**, *66* (9), 2911–2917.

(21) Stawiasz, K. J.; Wendell, C. I.; Suslick, B. A.; Moore, J. S. Photoredox-Initiated Frontal Ring-Opening Metathesis Polymerization. *ACS Macro Lett.* **2022**, 780–784.

(22) Crisenza, G. E. M.; Melchiorre, P. Chemistry Glows Green with Photoredox Catalysis. *Nat. Commun.* **2020**, *11* (1), 8–11.

(23) Tromp, M.; Van Bokhoven, J. A.; Van Haaren, R. J.; Van Strijdonck, G. P. F.; Van der Eerden, A. M. J.; Van Leeuwen, P. W. N. M.; Koningsberger, D. C. Structure-Performance Relations in Homogeneous Pd Catalysis by in Situ EXAFS Spectroscopy. *J. Am. Chem. Soc.* **2002**, *124* (50), 14814–14815.

(24) Streibel, V.; Velasco-Vélez, J. J.; Teschner, D.; Carbonio, E. A.; Knop-Gericke, A.; Schlögl, R.; Jones, T. E. Merging Operando and Computational X-Ray Spectroscopies to Study the Oxygen Evolution Reaction. *Curr. Opin. Electrochem.* **2022**, *35*, 101039.

(25) Singh, J.; Lamberti, C.; Bokhoven, J. A. V. Advanced X-Ray Absorption and Emission Spectroscopy: In Situ Catalytic Studies. *Chem. Soc. Rev.* **2010**, *39* (12), 4754–4766.

(26) Timoshenko, J.; Roldan Cuenya, B. In Situ/ Operando Electrocatalyst Characterization by X-Ray

Absorption Spectroscopy. *Chem. Rev.* **2021**, *121* (2), 882–961.

(27) Van Der Veen, R. M.; Milne, C. J.; Nahhas, A. El; Lima, F. A.; Pham, V. T.; Best, J.; Weinstein, J. A.; Borca, C. N.; Abela, R.; Bressler, C.; Chergui, M. Structural Determination of a Photochemieally Active Diplatinum Molecule by Time-Resolved EXAFS Spectroscopy. *Angew. Chemie - Int. Ed.* **2009**, *48* (15), 2711–2714.

(28) Van Der Veen, R. M.; Milne, C. J.; Pham, V. T.; El Nahhas, A.; Weinstein, J. A.; Best, J.; Borca, C. N.; Bressler, C.; Chergui, M. EXAFS Structural Determination of the $Pt_2(P_2O_5H_2)_4^{4-}$ Anion in Solution. *Chimia.* **2008**, *62* (4), 287–290.

(29) Rossi, T. C.; Dykstra, C. P.; Haddock, T. N.; Wallick, R.; Burke, J. H.; Gentle, C. M.; Doumy, G.; March, A. M.; Van Der Veen, R. M. Charge Carrier Screening in Photoexcited Epitaxial Semiconductor Nanorods Revealed by Transient X-Ray Absorption Linear Dichroism. *Nano Lett.* **2021**, *21* (22), 9534–9542.

(30) Gentle, C. M.; Wang, Y.; Haddock, T. N.; Dykstra, C. P.; van der Veen, R. M. Internal Atomic-Scale Structure Determination and Band Alignment of II–VI Quantum Dot Heterostructures. *J. Phys. Chem. C* **2020**, *124* (6), 3895–3904.

(31) van der Veen, R. M.; Kas, J. J.; Milne, C. J.; Pham, V.-T.; Nahhas, A. El; Lima, F. A.; Vithanage, D. A.; Rehr, J. J.; Abela, R.; Chergui, M. L-Edge XANES Analysis of Photoexcited Metal Complexes in Solution. *Phys. Chem. Chem. Phys.* **2010**, *12* (21), 5503–5513.

(32) Jay, R. M.; Kunnus, K.; Wernet, P.; Gaffney, K. J. Capturing Atom-Specific Electronic Structural Dynamics of Transition-Metal Complexes with Ultrafast Soft X-Ray Spectroscopy. *Annu. Rev. Phys. Chem.* **2022**, *73*, 187–208.

(33) Bergmann, U.; Kern, J.; Schoenlein, R. W.; Wernet, P.; Yachandra, V. K.; Yano, J. Using X-Ray Free-Electron Lasers for Spectroscopy of Molecular Catalysts and Metalloenzymes. *Nat. Rev.*

Phys. **2021**, *3*, 264–282.

(34) Zhao, J.; De Kreijger, S.; Troian-Gautier, L.; Yu, J.; Hu, W.; Zhang, X.; Elias, B.; Moonshiram, D. Deciphering the Photophysical Kinetics, Electronic Configurations and Structural Conformations of Iridium-Cobalt Hydrogen Evolution Photocatalysts. *Chem. Commun.* **2022**, *58* (58), 8057–8060.

(35) Norell, J.; Jay, R. M.; Hantschmann, M.; Eckert, S.; Guo, M.; Gaffney, K. J.; Wernet, P.; Lundberg, M.; Föhlisch, A.; Odelius, M. Fingerprints of Electronic, Spin and Structural Dynamics from Resonant Inelastic Soft X-Ray Scattering in Transient Photo-Chemical Species. *Phys. Chem. Chem. Phys.* **2018**, *20* (10), 7243–7253.

(36) Huse, N.; Cho, H.; Hong, K.; Jamula, L.; De Groot, F. M. F.; Kim, T. K.; McCusker, J. K.; Schoenlein, R. W. Femtosecond Soft X-Ray Spectroscopy of Solvated Transition-Metal Complexes: Deciphering the Interplay of Electronic and Structural Dynamics. *J. Phys. Chem. Lett.* **2011**, *2* (8), 880–884.

(37) Khalil, M.; Mukamel, S. Ultrafast Spectroscopy and Diffraction from XUV to X-Ray. *J. Chem. Phys.* **2020**, *153* (10), 20–23.

(38) Ismail, A. S. M.; Garcia-Torregrosa, I.; Vollenbroek, J. C.; Folkertsma, L.; Bomer, J. G.; Haarman, T.; Ghiasi, M.; Schellhorn, M.; Nachtegaal, M.; Odijk, M.; van den Berg, A.; Weckhuysen, B. M.; de Groot, F. M. F. Detection of Spontaneous FeOOH Formation at the Hematite/Ni(Fe)OOH Interface during Photoelectrochemical Water Splitting by Operando X-Ray Absorption Spectroscopy. *ACS Catal.* **2021**, *11* (19), 12324–12335.

(39) Chen, L. X.; Zhang, X.; Wasinger, E. C.; Lockard, J. V.; Stickrath, A. B.; Mara, M. W.; Attenkofer, K.; Jennings, G.; Smolentsev, G.; Soldatov, A. X-Ray Snapshots for Metalloporphyrin Axial Ligation. *Chem. Sci.* **2010**, *1* (5), 642–650.\

(40) Hong, J.; Kelley, M. S.; Shelby, M. L.; Hayes, D. K.; Hadt, R. G.; Rimmerman, D.; Zhang, X.; Chen, L. X. The Nature of the Long-Lived Excited State in a NiII Phthalocyanine Complex Investigated by X-Ray Transient Absorption Spectroscopy. *ChemSusChem* **2018**, *11* (14), 2421–2428.

(41) Hadt, R. G.; Hayes, D.; Brodsky, C. N.; Ullman, A. M.; Casa, D. M.; Upton, M. H.; Nocera, D. G.; Chen, L. X. X-Ray Spectroscopic Characterization of Co(IV) and Metal-Metal Interactions in Co4O4: Electronic Structure Contributions to the Formation of High-Valent States Relevant to the Oxygen Evolution Reaction. *J. Am. Chem. Soc.* **2016**, *138* (34), 11017–11030.

(42) Chergui, M.; Collet, E. Photoinduced Structural Dynamics of Molecular Systems Mapped by Time-Resolved X-Ray Methods. *Chem. Rev.* **2017**, *117* (16), 11025–11065.

(43) Chen, L. X. Taking Snapshots of Photoexcited Molecules in Disordered Media by Using Pulsed Synchrotron X-Rays. *Angew. Chemie - Int. Ed.* **2004**, *43* (22), 2886–2905.

(44) Penfold, T. J.; Milne, C. J.; Chergui, M. Recent Advances in Ultrafast X-Ray Absorption Spectroscopy of Solutions. *Adv. Chem. Phys.* **2013**, *153*, 1–41.

(45) Macmillan, S. N.; Lancaster, K. M. X-Ray Spectroscopic Interrogation of Transition-Metal-Mediated Homogeneous Catalysis: Primer and Case Studies. *ACS Catal.* **2017**, *7* (3), 1776–1791.

(46) Reischauer, S.; Strauss, V.; Pieber, B. Modular, Self-Assembling Metallaphotocatalyst for Cross-Couplings Using the Full Visible-Light Spectrum. *ACS Catal.* **2020**, *10* (22), 13269–13274.

(47) Gisbertz, S.; Reischauer, S.; Pieber, B. Overcoming Limitations in Dual Photoredox/Nickel-Catalysed C–N Cross-Couplings Due to Catalyst Deactivation. *Nat. Catal.* **2020**, *3* (8), 611–620.

(48) Duval, H.; Bulach, V.; Fischer, J.; Weiss, R. Four-Coordinate, Low-Spin (S = 0) and Six-Coordinate, High-Spin (S = 1) Nickel(II) Complexes of Tetraphenylporphyrins with β-Pyrrole Electron-Withdrawing Substituents: Porphyrin-Core Expansion and Conformation. *Inorg. Chem.*

1999, *38* (24), 5495–5501.

(49) Cotton, F. A.; Wilkinson, G. Advanced Inorganic Chemistry. John Wiley & Sons, Inc. 1999.

(50) Venanzi, L. M. Tetrahedral Complexes of Nickel (II) and the Factors Determining Their Formation. *J. Inorg. Nucl. Chem.* **1958**, *8* (C), 137–142. 1902(58)80175-X.

(51) Mink, H. J.; Schmidtke, H. H. Optical Properties of Ni[Tbu2P(O)NR]2. A Paramagnetic D8 Complex with Planar Structure. *Chem. Phys. Lett.* **1994**, *231* (2–3), 235–240.

(52) Shields, B. J.; Kudisch, B.; Scholes, G. D.; Doyle, A. G. Long-Lived Charge-Transfer States of Nickel(II) Aryl Halide Complexes Facilitate Bimolecular Photoinduced Electron Transfer. *J. Am. Chem. Soc.* **2018**, *140* (8), 3035–3039.

(53) Ting, S. I.; Garakyaraghi, S.; Taliaferro, C. M.; Shields, B. J.; Scholes, G. D.; Castellano, F. N.; Doyle, A. G. 3d-d Excited States of Ni(II) Complexes Relevant to Photoredox Catalysis: Spectroscopic Identification and Mechanistic Implications. *J. Am. Chem. Soc.* **2020**, *142*, (12), 5800-5810.

(54) Cagan, D. A.; Bím, D.; Silva, B.; Kazmierczak, N. P.; McNicholas, B. J.; Hadt, R. G. Elucidating the Mechanism of Excited-State Bond Homolysis in Nickel–Bipyridine Photoredox Catalysts. *J. Am. Chem. Soc.* **2022**, *144*, (14), 6516-6531.

(55) Kaizu, Y.; Ohta, H.; Kobayashi, K.; Kobayashi, H.; Takuma, K.; Matsuo, T. Lifetimes of the Lowest Excited State of Tris(2,2′-Bipyridine)Ruthenium(II) and Its Amphipathic Derivative in Micellar Systems. *J. Photochem.* **1985**, *30* (1), 93–103.

(56) Paulus, B. C.; Nielsen, K. C.; Tichnell, C. R.; Carey, M. C.; McCusker, J. K. A Modular Approach to Light Capture and Synthetic Tuning of the Excited-State Properties of Fe(II)-Based Chromophores. *J. Am. Chem. Soc.* **2021**, *143* (21), 8086–8098.

(57) Ma, P.; Wang, S.; Chen, H. Reactivity of Transition-Metal Complexes in Excited States: C-o Bond

Coupling Reductive Elimination of a Ni(Ii) Complex Is Elicited by the Metal-to-Ligand Charge Transfer State. *ACS Catal.* **2020**, *10* (1), 1–6.

(58) Dong, Y.; Zhao, Z.; Geng, Y.; Su, Z.; Zhu, B.; Guan, W. Theoretical Insight on the High Reactivity of Reductive Elimination of Ni. *Inorg. Chem.* **2023**, *62*, (3), 1156-1164.

(59) Welin, E. R.; Le, C.; Arias-Rotondo, D. M.; McCusker, J. K.; MacMillan, D. W. C. Photosensitized, Energy Transfer-Mediated Organometallic Catalysis through Electronically Excited Nickel(II). *Science* **2017**, *355* (6323), 380–385.

(60) Hong, J.; Fauvell, T. J.; Helweh, W.; Zhang, X.; Chen, L. X. Investigation of the Photoinduced Axial Ligation Process in the Excited State of Nickel(II) Phthalocyanine. *J. Photochem. Photobiol. A Chem.* **2019**, *372* 270–278.

(61) Phelan, B. T.; Mara, M. W.; Chen, L. X. Excited-State Structural Dynamics of Nickel Complexes Probed by Optical and X-Ray Transient Absorption Spectroscopies: Insights and Implications. *Chem. Commun.* **2021**, *57* (90), 11904–11921.

(62) Wernet, P. Chemical Interactions and Dynamics with Femtosecond X-Ray Spectroscopy and the Role of X-Ray Free-Electron Lasers. *Philos. Trans. R. Soc. A Math. Phys. Eng. Sci.* **2019**, *377* (2145).

(63) Al Samarai, M.; Hahn, A. W.; Beheshti Askari, A.; Cui, Y. T.; Yamazoe, K.; Miyawaki, J.; Harada, Y.; Rüdiger, O.; Debeer, S. Elucidation of Structure-Activity Correlations in a Nickel Manganese Oxide Oxygen Evolution Reaction Catalyst by Operando Ni L-Edge X-Ray Absorption Spectroscopy and 2p3d Resonant Inelastic X-Ray Scattering. *ACS Appl. Mater. Interfaces* **2019**, *11* (42), 38595–38605.

(64) Jay, R. M.; Vaz Da Cruz, V.; Eckert, S.; Fondell, M.; Mitzner, R.; Föhlisch, A. Probing Solute-Solvent Interactions of Transition Metal Complexes Using L-Edge Absorption Spectroscopy. *J.*

Phys. Chem. B **2020**, *124* (27), 5636–5645.

(65) Kubin, M.; Guo, M.; Ekimova, M.; Källman, E.; Kern, J.; Yachandra, V. K.; Yano, J.; Nibbering, E. T. J.; Lundberg, M.; Wernet, P. Cr L-Edge X-Ray Absorption Spectroscopy of CrIII(Acac)3 in Solution with Measured and Calculated Absolute Absorption Cross Sections. *J. Phys. Chem. B* **2018**, *122* (29), 7375–7384.

(66) Koroidov, S.; Hong, K.; Kjaer, K. S.; Li, L.; Kunnus, K.; Reinhard, M.; Hartsock, R. W.; Amit, D.; Eisenberg, R.; Pemmaraju, C. Das; Gaffney, K. J.; Cordones, A. A. Probing the Electron Accepting Orbitals of Ni-Centered Hydrogen Evolution Catalysts with Noninnocent Ligands by Ni L-Edge and S K-Edge X-Ray Absorption. *Inorg. Chem.* **2018**, *57* (21), 13167–13175.

(67) Miedema, P. S.; Quevedo, W.; Fondell, M. The Variable Polarization Undulator Beamline UE52 SGM at BESSY II. *J. large-scale Res. Facil. JLSRF* **2016**, *2*, 2–5.

(68) Fondell, M.; Eckert, S.; Jay, R. M.; Weniger, C.; Quevedo, W.; Niskanen, J.; Kennedy, B.; Sorgenfrei, F.; Schick, D.; Giangrisostomi, E.; Ovsyannikov, R.; Adamczyk, K.; Huse, N.; Wernet, P.; Mitzner, R.; Föhlisch, A. Time-Resolved Soft X-Ray Absorption Spectroscopy in Transmission Mode on Liquids at MHz Repetition Rates. *Struct. Dyn.* **2017**, *4* (5).

(69) Stavitski, E.; de Groot, F. M. F. The CTM4XAS Program for EELS and XAS Spectral Shape Analysis of Transition Metal L Edges. *Micron* **2010**, *41* (7), 687–694.

(70) Wang, H.; Ralston, C. Y.; Patil, D. S.; Jones, R. M.; Gu, W.; Verhagen, M.; Adams, M.; Ge, P.; Riordan, C.; Marganian, C. A.; Mascharak, P.; Kovacs, J.; Miller, C. G.; Collins, T. J.; Brooker, S.; Croucher, P. D.; Wang, K.; Stiefel, E. I.; Cramer, S. P. Nickel L-Edge Soft X-Ray Spectroscopy of Nickel-Iron Hydrogenases and Model Compounds - Evidence for High-Spin Nickel(II) in the Active Enzyme. *J. Am. Chem. Soc.* **2000**, *122* (43), 10544–10552.

(71) Krasnikov, S. A.; Preobrajenski, A. B.; Sergeeva, N. N.; Brzhezinskaya, M. M.; Nesterov, M. A.;

Cafolla, A. A.; Senge, M. O.; Vinogradov, A. S. Electronic Structure of Ni(II) Porphyrins and Phthalocyanine Studied by Soft X-Ray Absorption Spectroscopy. *Chem. Phys.* **2007**, *332* (2–3), 318–324.

(72) Groot, F. De. Multiplet Effects in X-Ray Spectroscopy. *Coord. Chem. Rev.* **2005**, *249* (1–2), 31–63.

(73) Ryland, E. S.; Zhang, K.; Vura-Weis, J. Sub-100 Fs Intersystem Crossing to a Metal-Centered Triplet in Ni(II)OEP Observed with M-Edge XANES. *J. Phys. Chem. A* **2019**, 123, (25), 5214-5222.

(74) Bridgeman, A. J. On the Origin of Paramagnetism in Planar Nickel(II) Complexes. *Dalt. Trans.* **2008**, *2* (15), 1989–1992.

(75) Evans, D. F. The Determination of the Paramagnetic Susceptibility. *J. Chem. Soc.* **1959**, 2003–2005.

(76) Bain, G. A.; Berry, J. F. Diamagnetic Corrections and Pascal's Constants. *J. Chem. Educ.* **2008**, *85* (4), 532–536.

(77) Cotton, F. A.; Goodgame, D. M. L. New Tetrahedral Complexes of Nickel(II). *J. Am. Chem. Soc. Soc.* **1960**, *82* (22), 5771–5774.

(78) Donoghue, J. T.; Drago, R. S. Non-Aqueous Coordination Phenomena -Complexes of Hexamethyl-Phosphoramide . I. Preparation and Properties of Tetrahedral $[Zn\{PO[N(CH_3)_2]_3\}_4]^{+2}$, $[Co\{PO[N(CH_3)_2]_3\}_4]^{+2}$, and $[Ni\{PO[N(CH_3)_2]_3\}_4]^{+2}$ Compounds. *Inorg. Chem.* **1962**, *1* (4), 866–872.

(79) Holm, R. H. Studies on Nickel(II) Complexes. II. On the Solution Magnetism of Bis-(N-Methylsalicylaldimine)-Nickel(II) and Related Complexes. *J. Chem. Soc.* **1961**, *83* (23), 4683–4690.

(80) Luca, O. R.; Konezny, S. J.; Paulson, E. K.; Habib, F.; Luthy, K. M.; Murugesu, M.; Crabtree, R. H.; Batista, V. S. Study of an S = 1 NiII Pincer Electrocatalyst Precursor for Aqueous Hydrogen Production Based on Paramagnetic 1H NMR. *Dalt. Trans.* **2013**, *42* (24), 8802–8807.

(81) Kahn, O. *Molecular Magnetism*; VCH Publishers, Inc., 1993.

(82) Desrochers, P. J.; Telser, J.; Zvyagin, S. A.; Ozarowski, A.; Krzystek, J.; Vicic, D. A. Electronic Structure of Four-Coordinate C3v Nickel(II) Scorpionate Complexes: Investigation by High-Frequency and -Field Electron Paramagnetic Resonance and Electronic Absorption Spectroscopies. *Inorg. Chem.* **2006**, *45* (22), 8930–8941.

(83) Howes, B. D.; Schiødt, C. B.; Welinder, K. G.; Marzocchi, M. P.; Ma, J. G.; Zhang, J.; Shelnutt, J. A.; Smulevich, G. The Quantum Mixed-Spin Heme State of Barley Peroxidase: A Paradigm for Class III Peroxidases. *Biophys. J.* **1999**, *77* (1), 478–492.

(84) Jay, R. M.; Norell, J.; Eckert, S.; Hantschmann, M.; Beye, M.; Kennedy, B.; Quevedo, W.; Schlotter, W. F.; Dakovski, G. L.; Minitti, M. P.; Hoffmann, M. C.; Mitra, A.; Moeller, S. P.; Nordlund, D.; Zhang, W.; Liang, H. W.; Kunnus, K.; Kubiček, K.; Techert, S. A.; Lundberg, M.; Wernet, P.; Gaffney, K.; Odelius, M.; Föhlisch, A. Disentangling Transient Charge Density and Metal-Ligand Covalency in Photoexcited Ferricyanide with Femtosecond Resonant Inelastic Soft X-Ray Scattering. *J. Phys. Chem. Lett.* **2018**, *9* (12), 3538–3543.

(85) Büchner, R.; Fondell, M.; Haverkamp, R.; Pietzsch, A.; Vaz da Cruz, V.; Föhlisch, A. The Porphyrin Center as a Regulator for Metal-Ligand Covalency and π Hybridization in the Entire Molecule. *Phys. Chem. Chem. Phys.* **2021**, *23* (43), 24765–24772.

(86) Van Kuiken, B. E.; Cho, H.; Hong, K.; Khalil, M.; Schoenlein, R. W.; Kim, T. K.; Huse, N. Time-Resolved X-Ray Spectroscopy in the Water Window: Elucidating Transient Valence Charge Distributions in an Aqueous Fe(II) Complex. *J. Phys. Chem. Lett.* **2016**.

(87) van Elp, J.; Peng, G.; Cramer, S. P.; Searle, B. G.; Mitra-Kirtley, S.; Huang, Y. H.; Johnson, K.; Zhou, Z. H.; Adams, M. W. W.; Maroney, M. J. Electronic Structure and Symmetry in Nickel L Edge X-Ray Absorption Spectroscopy: Application to a Nickel Protein. *J. Am. Chem. Soc.* **1994**, *116* (5), 1918–1923.

(88) Tian, L.; Till, N. A.; Kudisch, B.; MacMillan, D. W. C.; Scholes, G. D. Transient Absorption Spectroscopy Offers Mechanistic Insights for an Iridium/Nickel-Catalyzed C-O Coupling. *J. Am. Chem. Soc.* **2020**, *142* (10), 4555–4559.

(89) Kinigstein, E. D.; Jennings, G.; Kurtz, C. A.; March, A. M.; Zuo, X.; Chen, L. X.; Attenkofer, K.; Zhang, X. X-Ray Multi-Probe Data Acquisition: A Novel Technique for Laser Pump x-Ray Transient Absorption Spectroscopy. *Rev. Sci. Instrum.* **2021**, *92* (8).

(90) Smolentsev, G.; Soldatov, A. Quantitative Local Structure Refinement from XANES: Multi-Dimensional Interpolation Approach. *J. Synchrotron Radiat.* **2006**, *13* (1), 19–29.

(91) Shelby, M. L.; Lestrange, P. J.; Jackson, N. E.; Haldrup, K.; Mara, M. W.; Stickrath, A. B.; Zhu, D.; Lemke, H. T.; Chollet, M.; Hoffman, B. M.; Li, X.; Chen, L. X. Ultrafast Excited State Relaxation of a Metalloporphyrin Revealed by Femtosecond X-Ray Absorption Spectroscopy. *J. Am. Chem. Soc.* **2016**, *138* (28), 8752–8764.

(92) Joly, Y.; Bunu, O.; Lorenzo, J. E.; Galéra, R. M.; Grenier, S.; Thompson, B. Self-Consistency, Spin-Orbit and Other Advances in the FDMNES Code to Simulate XANES and RXD Experiments. *J. Phys. Conf. Ser.* **2009**, *190*.

(93) Bunău, O.; Joly, Y. Full Potential X-Ray Absorption Calculations Using Time Dependent Density Functional Theory. *J. Phys. Condens. Matter* **2012**, *24* (21).

(94) Campbell, L.; Tanaka, S.; Mukamel, S. Ligand Effects on the X-Ray Absorption of a Nickel Porphyrin Complex: A Simulation Study. *Chem. Phys.* **2004**, *299* (2–3), 225–231.